

Joint effects of genes underlying a temperature specialization tradeoff in yeast

Faisal AlZaben¹, Julie N. Chuong^{1,2}, Melanie B. Abrams¹, and Rachel B. Brem¹

¹Department of Plant and Microbial Biology, UC Berkeley, Berkeley, CA

²Current address: Ph.D. Program in Biology, New York University, New York, NY

1 Abstract

2 A central goal of evolutionary genetics is to understand, at the molecular level, how organisms adapt to their
3 environments. For a given trait, the answer often involves the acquisition of variants at unlinked sites across
4 the genome. Genomic methods have achieved landmark successes in pinpointing adaptive loci. To figure out
5 how a suite of adaptive alleles work together, and to what extent they can reconstitute the phenotype of
6 interest, requires their transfer into an exogenous background. We studied the joint effect of adaptive, gain-of-
7 function thermotolerance alleles at eight unlinked genes from *Saccharomyces cerevisiae*, when introduced into
8 a thermosensitive sister species, *S. paradoxus*. Although the loci damped each other's beneficial impact (that
9 is, they were subject to negative epistasis), most boosted high-temperature growth alone and in combination,
10 and none was deleterious. The complete set of eight genes was sufficient to confer ~15% of the *S. cerevisiae*
11 phenotype in the *S. paradoxus* background. The same loci also contributed to a heretofore unknown
12 advantage in cold growth by *S. paradoxus*. Together, our data establish temperature resistance in yeasts as a
13 model case of a genetically complex evolutionary tradeoff, which can be partly reconstituted from the
14 sequential assembly of unlinked underlying loci.

15 Author summary

16 Organisms adapt to threats in the environment by acquiring DNA sequence variants that tweak traits to
17 improve fitness. Experimental studies of this process have proven to be a particular challenge when they
18 involve manipulation of a suite of genes, all on different chromosomes. We set out to understand how so many
19 loci could work together to confer a trait. We used as a model system eight genes that govern the ability of the
20 unicellular yeast *Saccharomyces cerevisiae* to grow at high temperature. We introduced these variant loci
21 stepwise into a non-thermotolerant sister species, and found that the more *S. cerevisiae* alleles we added, the
22 better the phenotype. We saw no evidence for toxic interactions between the genes as they were combined.
23 We also used the eight-fold transgenic to dissect the biological mechanism of thermotolerance. And we
24 discovered a tradeoff: the same alleles that boosted growth at high temperature eroded the organism's ability

25 to deal with cold conditions. These results serve as a case study of modular construction of a trait from nature,
26 by assembling the genes together in one genome.

27 Introduction

28 Understanding how organisms acquire new traits is a driving question in evolutionary biology. Many traits of
29 interest are adaptations, meaning they provide a fitness benefit to the organism which has driven their rise to
30 high frequency in the population. Genomic methods often find a slew of unlinked changes at the DNA level that
31 associate with a given adaptive trait (Burke and Rose, 2009; Iranmehr et al., 2021; Pardo-Diaz et al., 2015;
32 Sella and Barton, 2019). For any one candidate locus, gold-standard validation experiments will then swap
33 alleles between taxa and test for an impact on phenotype, at genic (Castro et al., 2019; Chan et al., 2010;
34 Kryazhimskiy et al., 2014; Linnen et al., 2013, 2009; Xie et al., 2019) and sub-genic (Anderson et al., 2016;
35 Bridgham et al., 2009; Escudero et al., 2020; Finnigan et al., 2012; Lindsey et al., 2013; Liu et al., 2018;
36 Palmer et al., 2015, 2015; Pillai et al., 2020; Toprak et al., 2011; Weinreich et al., 2006) levels of resolution.
37 Though elegant and rigorous, this focused approach on a given gene will by necessity leave polygenic
38 mechanisms of the trait less well characterized.

39 For a more complete picture of a complex adaptation, we would establish how multiple underlying genes work
40 together, including their interdependence and their joint ability to recapitulate the phenotype. Such questions
41 have come within reach in laboratory evolution, with particular emphasis on genomic inferences of epistasis
42 between unlinked adaptive loci (Aggeli et al., 2020; Blount et al., 2012; Bons et al., 2020; Buskirk et al., 2017;
43 Csilléry et al., 2018; Fisher et al., 2019; Good et al., 2017; Johnson et al., 2021; Kryazhimskiy et al., 2014;
44 Weber et al., 1999). In a handful of cases, adaptive multi-gene interactions from a lab evolution have been
45 verified experimentally by allelic replacement (Chou et al., 2011; Khan et al., 2011). To date, validating these
46 principles in the context of evolution from the wild has posed a key challenge (although see Marcusson et al.,
47 2009; Neverov et al., 2015; Roop et al., 2016).

48 To study complex genetic mechanisms in adaptation, we set out to use natural variation in *Saccharomyces*
49 yeasts as a model. *S. cerevisiae* strains, from the wild and the lab, grow at temperatures up to 41°C

(Gonçalves et al., 2011; Salvadó et al., 2011; Sweeney et al., 2004). All other species in the *Saccharomyces* clade, which diverged from a common ancestor ~20 million years ago, grow poorly at high temperatures, though many outperform *S. cerevisiae* in the cold (Hittinger, 2013). In previous work (Weiss et al., 2018) we developed a genomic version of the reciprocal hemizyosity test to dissect thermotolerance, using *S. paradoxus*, the closest sister species to *S. cerevisiae*, as a representative of the inferred ancestral state. Derived alleles of the mapped genes in *S. cerevisiae*, when tested individually for their marginal effects, were partially necessary or sufficient for thermotolerance, or both (Weiss et al., 2018), and their sequences exhibit evidence for positive selection in *S. cerevisiae* (Abrams et al., 2021; Weiss et al., 2018). But how these genes work together has remained unknown. We thus aimed to investigate the extent to which unlinked thermotolerance loci assembled in the same background would explain the trait, and whether and how these genes would depend on one another for their effects. We expected that any answers could also help elucidate other facets of the mechanism and the evolutionary history of thermotolerance.

Results

Combining thermotolerance loci to reconstitute a complex trait

We previously mapped eight genes with pro-thermotolerance alleles in *S. cerevisiae* (Table 1; Weiss et al., 2018). To explore the joint function of these unlinked loci, we introduced the alleles of all eight from DBVPG1373, a soil isolate of *S. cerevisiae* from the Netherlands, into Z1, a strain of the sister species *S. paradoxus*, isolated from an English oak tree (Liti et al., 2009). Our approach used a stepwise set of gene replacements. With CRISPR/Cas9 we introduced the *S. cerevisiae* allele of the promoter and coding region of a given gene into the endogenous location in wild-type *S. paradoxus*; we used the resulting strain as a background for the replacement of the *S. paradoxus* allele of the next gene by that of *S. cerevisiae*; and so on until all eight genes were swapped into one genome (Figure 1, bottom).

We first assayed growth of the eight-gene transgenic and the wild-type parental species at 39°C, with biomass accumulation (growth efficiency; the increase in optical density after 24 hours relative to that at the start) as a readout of strain performance. The results revealed an advantage of 2.07-fold attributable to the eight *S.*

75 *cerevisiae* alleles in the *S. paradoxus* background (Figure 1, inset and Table S1A), and no such effect in 28°C
76 control conditions (Figure S1). This joint phenotype recapitulated 15% of the trait divergence between wild-type
77 *S. cerevisiae* and *S. paradoxus* at 39°C (Figure 1, inset), with comparable results at temperatures down to
78 37°C (Figure S2). These data make clear that the full genetic architecture of *S. cerevisiae* thermotolerance
79 must involve more loci than the eight we have manipulated here—highlighting the potential for high genetic
80 complexity of this trait divergence between species.

81 **Negative epistasis among thermotolerance genes**

82 We hypothesized that *S. cerevisiae* thermotolerance determinants might depend on one another to confer their
83 effects. We sought to test this at the whole-gene level, treating the allele of each thermotolerance locus
84 (including the promoter and coding region) as a module, and investigating the interactions between them. The
85 *S. cerevisiae* allele of each module, when introduced on its own into *S. paradoxus*, was sufficient for a <1.4-
86 fold benefit in biomass accumulation at 39°C, as expected (Figure S3 and Weiss et al., 2018). We summed
87 these measurements to yield an expected phenotype under the assumption of independent gene function,
88 which we compared to the true measurement from the *S. paradoxus* strain harboring all eight thermotolerance
89 loci from *S. cerevisiae*. The latter came in significantly below the estimate from the model assuming
90 independence (Figure 2A). Thus, the combination of all eight genes was subject to negative epistasis,
91 improving growth at high temperature to an extent less than the sum of its parts.

92 We next turned to the strains we had made in the service of the eight-gene transgenic. These harbored *S.*
93 *cerevisiae* modules of one thermotolerance gene in the *S. paradoxus* background, two genes, three genes,
94 and so on (Figure 1, bottom). We considered this strain panel as an arbitrary trajectory through a gene-wise
95 genetic landscape from the *S. paradoxus* wild-type to the eight-locus swap. Though it represented just one of
96 tens of thousands of possible paths, we anticipated that it could help inform our understanding of the genetic
97 architecture of thermotolerance.

98 In assays of biomass accumulation at 39°C in each strain of the panel, we saw a generally monotonic
99 relationship between thermotolerance and the number of *S. cerevisiae* gene modules introduced into *S.*

100 *paradoxus* (Figure 1 and Table S1A). No such pattern emerged from a 28°C control (Figure S1 and Table
101 S1B). For a quantitative analysis, we converted the phenotypic profiles in the strain set to effect sizes, each
102 reporting the impact of the *S. cerevisiae* allele of a gene on thermotolerance, in the chimeric background into
103 which it was introduced (Figure 2B). Inspection of this metric confirmed that each *S. cerevisiae* gene addition
104 boosted the phenotype along the path to the eight-fold transgenic, in most cases significantly so (Table S1A),
105 with one exception. The pro-thermotolerance function of *S. cerevisiae* *SCC2*, discernable when it was
106 introduced on its own into *S. paradoxus* (Figure S3), was either below our detection limit or absent altogether
107 in combination with *S. cerevisiae* *DYN1* and *MYO1* (Figures 1 and 2B). Despite this potential case of masking
108 epistasis, the remaining trend for beneficial effects by *S. cerevisiae* alleles as we built up the eight-locus strain
109 was highly non-random (binomial $p = 0.03$). In no case did we observe a defect from swapping in an *S.*
110 *cerevisiae* allele, meaning we had no evidence for sign epistasis in this system.

111 We also used our multi-genic strain panel, alongside single-gene transgenics in *S. paradoxus*, to compare *S.*
112 *cerevisiae* allele-replacement effects across backgrounds. In most cases, a given thermotolerance gene from
113 *S. cerevisiae* had less impact in the presence of other *S. cerevisiae* loci than when tested on its own in *S.*
114 *paradoxus* (Figure 2B). This finding confirmed the negative (magnitude) epistasis between the *S. cerevisiae*
115 alleles of thermotolerance genes that we had inferred with the eight-gene transgenic (Figure 2A). We noted
116 that the damping of allelic effect by genetic background was most apparent at thermotolerance genes
117 annotated in chromosome segregation/mitosis (*DYN1*, *MYO1*, *SCC2*, *APC1*, and *ESP1*; Figure 2B). By
118 contrast, introducing the *S. cerevisiae* allele of *TAF2* or *AFG2*, involved in transcription and translation
119 respectively, drove nearly the same benefit on its own in *S. paradoxus* and in the respective multi-swap
120 chimera (Figure 2B).

121 Together, these genetic data characterize an example path toward thermotolerance of incremental advances
122 from *S. cerevisiae* gene modules—most limiting each other's effects to some extent, but without frank
123 deleterious consequences.

124 **Thermotolerance loci improve viability only during active growth**

125 We next aimed to investigate cellular mechanisms of thermotolerance, using as a tool the strain with all eight of
126 our focal genes from *S. cerevisiae* replaced into *S. paradoxus*. We focused on cell viability, as assayed by
127 counts of colony-forming units (CFUs) from aliquots of liquid culture at 39°C. In a first characterization of strain
128 performance in growing cultures under this setup, *S. paradoxus* cells were much less viable than those of *S.*
129 *cerevisiae*, across a range of warm temperatures (Figure S4), as expected. We anticipated that *S. cerevisiae*
130 alleles of our thermotolerance loci would rescue this phenotype, at least in part. This prediction bore out in our
131 CFU assays from actively growing cultures: at 39°C, the eight-gene transgenic survived 7-fold better than did
132 its *S. paradoxus* progenitor (Figure 3A). An analogous test of wild-type *S. cerevisiae* revealed three logs higher
133 viability than that of *S. paradoxus* during active growth at 39°C (Figure 3A).

134 The poor performance of strains of *S. paradoxus* origin in the CFU assay (Figure 3A) was much bigger in
135 magnitude than that seen in our measurements of biomass accumulation (Figure 1), in growing cultures. Such
136 a discrepancy suggests that some cells with *S. paradoxus* genotypes manage to divide early in the heat
137 treatment and then ultimately die, contributing at the end of the incubation to measured biomass but not
138 viability. Qualitatively, however, both experiments led to the same conclusion: *S. cerevisiae* alleles of
139 thermotolerance loci recapitulate part but not all of the advantage by *S. cerevisiae* relative to *S. paradoxus*
140 during active growth at 39°C. We detected no viability differences between strains during active growth at 28°C
141 (Figure S5A).

142 To gain insight into why *S. paradoxus* cells die at high temperature, we took account of the role in mitosis for
143 most of our thermotolerance genes (Table 1). We hypothesized that failure of the *S. paradoxus* cell growth
144 machinery was the proximal cause of death for this species at 39°C. If so, we expected that the underlying
145 alleles would not be a liability if cells did not enter the cell cycle in the first place. As a test of this notion, we
146 retooled our viability assay to start by incubating a liquid culture at a permissive temperature until it reached
147 stationary phase (when nutrients are exhausted and cell division arrests). We then switched these non-growing
148 cultures to 39°C, and finally took aliquots for assays of CFUs. The results revealed that, when exposed to heat
149 as a stationary-phase culture, *S. paradoxus* survived nearly as well as did *S. cerevisiae* (Figure 3B), in contrast
150 to the many logs of difference between the species during active growth (Figure 3A). Likewise, transgenesis of

our eight thermotolerance genes had no impact on high temperature survival in stationary phase (Figure 3B). Viability experiments on stationary-phase cultures at 28°C also found no difference between strains (Figure S5B).

These viability data show that the thermotolerance defect of *S. paradoxus* alleles from our eight-gene transgenic strain only manifests in actively growing cells, consistent with the hallmarks of cell cycle breakdown seen in microscopy assays of *S. paradoxus* at 39°C (Weiss et al., 2018). Together, our results support a model in which passage through mitosis itself is lethal at high temperature for *S. paradoxus*, whereas cells in an arrested state are protected from damage and death. *S. cerevisiae*, meanwhile, grows and divides successfully at 39°C, owing in part to its thermotolerant mitotic genes.

An evolutionary tradeoff in tolerance of extreme temperatures

Given that *S. cerevisiae* is unique within its clade for its ability to grow at high temperatures, we anticipated that this trait could have evolved as part of a tradeoff, and that cold tolerance would be a logical potential opposing character. Consistent with this picture, we observed generally better cold resistance across a panel of wild *S. paradoxus* relative to environmental isolates of *S. cerevisiae* (Figure S6). No such difference is detectable at 28°C (Weiss et al., 2018). We reasoned that thermotolerance alleles at our eight focal genes could contribute to the poor growth by *S. cerevisiae* in the cold. Indeed, our eight-fold transgenic strain grew significantly worse than did wild-type *S. paradoxus* at 4°C (Figure 4). With respect to biomass accumulation, this strain recapitulated 15% of the divergence between the wild-type species at 4°C—paralleling the analogous quantity at 39°C (Figure 1), and establishing antagonistic pleiotropy by *S. cerevisiae* alleles at our focal genes.

We hypothesized that thermotolerance loci could contribute to growth in the cold by mechanisms that would differ from the genetics we had elucidated at high temperature. In analysis of individual genes, only the *S. cerevisiae* allele of *DYN1* reduced biomass accumulation markedly at 4°C when introduced into *S. paradoxus* on its own, though a number of other genes had smaller effects (Figure S7). Likewise, across our panel of combinatorial gene replacements, most strains roughly phenocopied the single-gene *DYN1* swap in terms of growth efficiency (Figure S8). This contrasted with the stairstep-like trend of increasing thermotolerance as *S.*

176 *cerevisiae* alleles were stacked in the *S. paradoxus* background (Figure 1). We thus considered *DYN1* as a
177 central player in the cold sensitivity of *S. cerevisiae*, against a backdrop of more subtle contributions from other
178 loci, alone and in combination.

179 In viability assays during growth at 39°C, we had found robust divergence in survival between *S. cerevisiae*
180 and *S. paradoxus*, as well as survival effects of variation at our thermotolerance loci (Figure 3A). It remained
181 an open question whether the genetics of cold tolerance would have effects on cell death. In viability assays
182 we saw very little difference between *S. cerevisiae*, *S. paradoxus*, and our eight-gene transgenic in the *S.*
183 *paradoxus* background, in terms of CFUs after incubation at 4°C (Figure S9). This result underscores the
184 difference in mechanism between cryotolerance and thermotolerance in this system, and establishes that *S.*
185 *cerevisiae* alleles (at thermotolerance loci and others) slow growth in the cold rather than killing cells outright.

186 Discussion

187 Evolution often uses variants at genes scattered throughout the genome to build an adaptive trait. The
188 complete set of these loci, once in hand, can reconstitute the trait in an exogenous background, which is the
189 ultimate goal for many biomedically and industrially relevant characters. Along the way, the underlying genes
190 can shed light on the process by which a trait arose, which may involve events from millions of years ago. In
191 this work, we have used thermotolerance, a model fitness-relevant character whose underlying genes have
192 been under positive selection in environmental isolates of *S. cerevisiae* (Abrams et al., 2021; Weiss et al.,
193 2018), to explore genetic, biological, and evolutionary mechanisms of adaptation.

194 Introducing eight unlinked genes from *S. cerevisiae* into *S. paradoxus*, we reconstituted ~15% of the difference
195 in thermotolerance between the respective purebred species. Much of the architecture for this trait thus
196 remains unmapped, likely due in part to limitations of coverage and power in our original reciprocal
197 hemizyosity scan (Weiss et al., 2018), and to its restriction to the nuclear genome. Incisive experiments have
198 established the role of mitotype in temperature tolerance as it differs between *S. cerevisiae* and either *S.*
199 *paradoxus* or a farther-diverged species of the complex, *S. uvarum* (Baker et al., 2019; Hewitt et al., 2020; Li et
200 al., 2019; Špírek et al., 2014). Thus, mitochondrial variants presumably make up much of the heritability

201 missing from our current gene set. And *S. cerevisiae* alleles of the nuclear-encoded genes that we study here
202 could well depend on the *S. cerevisiae* mitochondrial genome for their full effect.

203 In our focus on nuclear-encoded thermotolerance factors, we found that most *S. cerevisiae* alleles improved
204 high-temperature growth, when tested on their own in *S. paradoxus* or in a chimeric multi-swap background. In
205 principle, these effects could be limited by partial incompatibilities in *S. paradoxus*—*i.e.* a given gene could
206 have made an even bigger contribution to thermotolerance in the presence of other functional partners from *S.*
207 *cerevisiae*. Even in such a case, the qualitative conclusion from our own data would remain: *S. cerevisiae*
208 alleles mostly help and do not hurt at high temperature, alone or combined. This profile provides an intriguing
209 contrast to the sign epistasis often detected between adaptive amino acid changes within a given protein, as
210 they boost fitness in some combinations and exert a frank defect in others (Starr and Thornton, 2016;
211 Weinreich et al., 2005). Since we have not surveyed all possible subsets of our mapped thermotolerance
212 genes, and more remain unidentified, we cannot rule out the possibility of toxic interactions at high temperature
213 between some *S. cerevisiae* versions of unlinked loci when they come together. That said, our thermotolerance
214 data as they stand conform to the idea that combining adaptive variants across unlinked sites will be less
215 constrained than, say, repacking a given protein (Toprak et al., 2011). This model is especially compelling in
216 the search to understand evolutionary dynamics in sexual systems. If a gene module can recombine into most
217 backgrounds and confer a benefit, it would speed the advance toward fitness of the population as a whole.

218 We found that the magnitude of the phenotypic effect of our focal genes depended on genetic background. For
219 our analyses of epistasis, we focused on thermotolerance, under the assumption that this trait or its correlates
220 have mattered for fitness in wild *S. cerevisiae*, and thus that genetic interactions could have been at play
221 during the adaptation process. We found ample evidence for negative epistasis, with the *S. cerevisiae* alleles
222 of some of our unlinked loci obscuring the thermotolerance effects of others, in replacements into *S.*
223 *paradoxus*. Negative epistasis has been a linchpin of classical genetic studies placing unlinked loss-of-function
224 mutants in pathways (Avery and Wasserman, 1992; Roth et al., 2009), and their genomic equivalent, reverse-
225 genetic double-mutant screens (Baryshnikova et al., 2013; Shen et al., 2017; Tutuncuoglu and Krogan, 2019;
226 Wong et al., 2016). Negative epistasis also features in the polygenic architectures of putatively neutral and

disease traits that vary in populations (Gusareva and Van Steen, 2014; Mackay, 2014; Ritchie, 2015). Our thermotolerance system complements these scenarios, in that we focus on alleles that act as gains of function, at least at high temperature (Weiss et al., 2018). Under the latter condition, we detected the most marked negative epistasis among thermotolerance genes with annotations in chromosome segregation and cell division. We can speculate that the *S. cerevisiae* allele at any such locus, as it rescues one aspect of cell division at 39°C, also pulls up the function of other parts of the mitotic machinery to some extent, e.g. by stabilizing heteromeric protein complexes. *S. cerevisiae* alleles of additional genes, introduced into such a background, would make less dramatic improvements to the phenotype than would be expected from their respective single-gene allele-swap strains.

Importantly, a sizeable literature has described negative epistasis between unlinked adaptive loci in laboratory evolution experiments, especially in microbes (Aggeli et al., 2020; Blount et al., 2012; Bons et al., 2020; Buskirk et al., 2017; Csilléry et al., 2018; Fisher et al., 2019; Good et al., 2017; Johnson et al., 2021; Kryazhimskiy et al., 2014; Tenaillon et al., 2012; Weber et al., 1999), where suites of unlinked variants have been validated in terms of effects on fitness (Chou et al., 2011; Khan et al., 2011). A chief emphasis here has been on evolutionary dynamics, in that negative epistatic interactions limit the availability of mutational steps with big fitness effects that would otherwise speed adaptation (Starr and Thornton, 2016; Weinreich et al., 2005). This principle plays out in part through diminishing-returns epistasis (Kryazhimskiy et al., 2014; Wisser et al., 2013), the difficulty of improving the fitness of somewhat-fit backgrounds, which can be explained by heightened susceptibility of fast-growing strains to pleiotropic effects of new mutations (Johnson et al., 2019). Though the latter has been a landmark of the recent literature, we do not consider it an immediately relevant model for our own data because of our focus on backgrounds that perform very poorly at 39°C. In more advanced stages of an allele-swap progression, which would reconstitute more of the yeast thermotolerance phenotype, we would expect genes to interact under the diminishing-returns mechanism.

Along with our insights into the genetics of thermotolerance, we discovered a cold resistance defect in *S. cerevisiae* relative to *S. paradoxus*, complementing previous temperature profiling using other assays across the genus (Hittinger, 2013; Salvadó et al., 2011). And we were able to pinpoint the genetic basis of this

phenotype, at least in part, to pro-thermotolerance *S. cerevisiae* alleles at our focal genes. The latter could be attributed largely to *S. cerevisiae* *DYN1*, which elicited the most dramatic drop in cold tolerance when tested on its own in *S. paradoxus*, and overshadowed the effects of other loci in multi-gene swap backgrounds. This echoes the known breakdown of *S. cerevisiae* *DYN1* protein function below 8°C, as distinguished from the mammalian ortholog (Hong et al., 2016). The emerging picture is that *S. cerevisiae* harbors alleles of *DYN1* (and other genes) that have been adaptive in its ancestral niche and yet act as a liability in the cold; other deleterious effects could also be at play, in conditions beside those studied here. Given that *S. cerevisiae* also tolerates ethanol better than the rest of its clade (Herbst et al., 2017; Williams et al., 2015), one appealing model posits that its unique ability to ferment drove *S. cerevisiae*'s origin as a species (Goddard, 2008), generating heat and ethanol at levels that kill off its microbial competitors. If so, our data strongly suggest that *S. cerevisiae* could not achieve this adaptation as a temperature generalist, and had to make a tradeoff by acquiring alleles that eroded the capacity to deal with cold.

Acknowledgements

The authors thank Dmitri Petrov for motivating the analysis of the thermotolerance of stationary-phase cultures; Abel Duarte and Jeff Skerker for direction and advice with molecular biology; Carly Weiss and Jeremy Roop for other helpful discussions; and David Savage for his generosity with lab facilities and resources.

Methods

Strain construction

Strains used in this work are listed in Table S3. To study combinations of *S. cerevisiae* alleles in an *S. paradoxus* background, we used as the latter the wild-type homozygous diploid *S. paradoxus* Z1, originally isolated from tree bark in the UK (Liti et al., 2009). We used our CRISPR/Cas9 method (Weiss et al., 2018), essentially as described but with slight modifications detailed below, to replace both copies of a given thermotolerance locus, at the endogenous location, with the allele from *S. cerevisiae* DBVPG1373, a soil isolate from the Netherlands (Liti et al., 2009). To build the eight-gene transgenic, we started with the single-

277 gene transgenic in the Z1 background harboring the *S. cerevisiae* allele of *DYN1* from Weiss et al., 2018. We
278 introduced *S. cerevisiae* alleles at additional genes in an iterative series of transformations; after each, we
279 cultured an isogenic stock from a single colony for Sanger sequence confirmation and storage, and, where
280 appropriate, we used this stock as input into the next transformation.

281 A given transformation involved donor DNA and constructs encoding guide RNAs for Cas9 to target
282 replacement of the *S. paradoxus* allele with that from *S. cerevisiae* at either one or two loci, which Sanger
283 sequencing then verified to be successful at one or both. For each locus we used designs of guide RNAs from
284 Weiss et al., 2018 that targeted, for double-strand breaks, the endogenous Z1 allele by Cas9; one guide
285 targeted a site ~1000bp upstream of the coding start of the gene of interest (or the 3' end of the closest
286 upstream gene) in the Z1 genome and the other guide targeted a site near the coding stop. Cas9 editing
287 proceeded as described (Weiss et al., 2018). Briefly, for each transformation step of strain construction, one or
288 two guide RNA pairs, targeting one or two loci respectively, were cloned into plasmid pBC712, which also
289 encodes *Streptococcus pyogenes* Cas9. Next, DNA to serve as a repair template was generated for each
290 relevant locus, via PCR from *S. cerevisiae* DBVPG1373, with 90bp primers that contained 70bp of sequence
291 homologous to *S. paradoxus* Z1 on each side of the amplified DNA product. Finally, plasmid and repair
292 template were transformed into the Z1 descendant as described (Weiss et al., 2018) at a ratio of 0.3 to 3.5
293 based on the length of the donor DNA, equivalent to 10^{12} dsDNA molecules for 10 μ g of plasmid. Putative
294 transformants were purified and sequence-verified.

295 **Growth assays**

296 Measurements of biomass accumulation (growth efficiency) at 39°C in Figure 1 were done essentially as
297 described (Weiss et al., 2018) with modifications as follows. For a given day's worth of experiments, wild-type
298 *S. paradoxus* Z1 and one or more other strains of interest were streaked onto a yeast peptone dextrose (YPD)
299 plate from a -80°C freezer stock and incubated at 28°C for 2 days. 2-8 colonies of a given strain were each
300 inoculated separately in 5mL of liquid YPD and grown for 24 hours at 28°C with shaking at 200rpm to
301 saturation; we refer to the cultures at this stage as pre-cultures. Each such replicate pre-culture was back-
302 diluted into 10mL of YPD to achieve an OD₆₀₀ of 0.05; incubated at 28°C until it reached an OD₆₀₀ of 0.4-0.8;

303 back-diluted again to OD_{600} of to achieve an OD_{600} of 0.1; and then incubated for 24 hours at 39°C. We
304 tabulated the difference in OD_{600} between the final and initial timepoints across this 24-hour incubation for each
305 culture. This procedure, from streaking on solid medium through inoculation, heat treatment, and biomass
306 measurement, was repeated at least four times for each strain in the analysis of Figure 1. The resulting vector
307 of biomass measurements across all replicates from all days for each strain was compared to that for each
308 other strain with a one-tailed Wilcoxon test in Table S1. Multiple testing was corrected for using the Benjamini-
309 Hochberg method.

310 Measurements of biomass accumulation at 28°C in Figure S1 were done as described (Weiss et al., 2018).
311 Strains were streaked on solid plates and one colony per strain was pre-cultured in liquid at 28°C as above.
312 Each such saturated pre-culture was back-diluted to achieve an OD_{600} of 0.05 and grown for an additional 5.5
313 hours at 28°C until it reached logarithmic phase. We transferred cells from each such pre-culture, and YPD, to
314 five replicate wells of a 96-well plate, with volumes sufficient to yield a total volume of 150 μ L per well at an
315 OD_{600} of 0.02. The plate was covered with a gas-permeable membrane (Sigma) and incubated with orbital
316 shaking in an M200 plate reader (Tecan, Inc.) at 28°C for 24 hours. We tabulated the difference in OD_{600}
317 between the final and initial timepoints across this 24-hour incubation for each replicate culture. The vector of
318 these replicate measurements for each strain was compared to that from *S. paradoxus* with a two-tailed
319 Wilcoxon test. Multiple testing was corrected for using the Benjamini-Hochberg method.

320 For measurements of biomass accumulation at 37°C - 39°C in Figure S2, strains were streaked, and three
321 colonies of a given strain were pre-cultured in liquid as above. Each such replicate liquid culture was back-
322 diluted into 10mL of YPD to achieve an OD_{600} of 0.05; incubated at 28°C until it reached an OD_{600} of 0.4-0.8;
323 back-diluted again to OD_{600} of to achieve an OD_{600} of 0.1; and then incubated for 24 hours at the temperature
324 of interest. We tabulated the difference in OD_{600} between the final and initial timepoints across this 24-hour
325 incubation for each replicate culture. The vector of these replicate measurements for each strain at a given
326 temperature was compared to that from *S. paradoxus* with a one-tailed Wilcoxon test. In Figure S2, lines are
327 the result of a polynomial regression on the points, created using Seaborn's regplot in Python 3.7.

328 For measurements of growth at 4°C in Figure 4 and Figures S6-S8, for a given day's worth of experiments,
329 strains were streaked on solid plates and three to eight colonies per genotype, respectively, were pre-cultured
330 in liquid, each as an independent biological replicate, as above. After the second back-dilution, each liquid
331 culture was incubated for 11 days at 4°C in a rotating shaker at maximum speed in a cold room. The OD₆₀₀
332 was measured on days 0, 4, 5, 7, 8, 9, 10, and 11, and also on day 6 for Figures S6-S8. To measure biomass
333 accumulation (growth efficiency) we tabulated the difference in OD₆₀₀ between the final and initial timepoints
334 across this 11-day incubation for each replicate culture. Two such days' worth of experiments were carried out
335 for each strain in Figures S7 and S8, and one in Figures 4 and S6. We collated the measurements from all
336 replicate culture measurements across all days for a given strain and compared each transgenic against *S.*
337 *paradoxus* with a one-tailed Wilcoxon test. Separately, we fit a logistic curve to the timecourse measurements
338 for each replicate using Scipy's `curve_fit` function as a part of Scipy's `optimize` package (Python 3.7). Bounds
339 for the parameters of the logistic equation (the carrying capacity, growth rate, and time to half-maximal growth)
340 were constrained to the range -1.0 to 10.0, and the Trust Region Reflective algorithm was used to find the best
341 fit. We collated the growth rate estimates from all replicate culture measurements across all days for a given
342 strain and compared each transgenic against *S. paradoxus* with a one-tailed Wilcoxon test.

343 **Viability assays**

344 For the survey of viability phenotypes at high temperatures across environmental isolates in Figure S4, strains
345 were streaked out and four colonies of each were pre-cultured in liquid as for 39°C growth above, except that
346 the initial pre-culture to achieve saturation lasted 48 hours. Each pre-culture was back-diluted into 10 mL of
347 YPD to reach an OD₆₀₀ of 0.05 and then cultured for 24 hours at the temperature of interest (35°C - 38°C). The
348 OD₆₀₀ at the end of this timecourse was measured for each such replicate culture. Then to measure viability for
349 each, we diluted aliquots from the culture in a 1:10 series and spotted 3μL of each dilution for growth on a solid
350 YPD plate. After incubation at 28°C for two days, we used the dilution corresponding to the most dense spot
351 that was not a lawn for the final report of viability: we counted the number of colonies in each of the two
352 technical replicate spots, formulated the number of colony-forming units per mL of undiluted culture (CFU/mL),
353 and divided this ratio by the OD₆₀₀ we had measured at the end of the liquid timecourse, to account for

354 differences in the number of dead cells that contribute to the latter. At a given temperature, the vector of
355 viability measurements across all replicate liquid cultures for all *S. cerevisiae* strains was compared to that for
356 all *S. paradoxus* strains with a one-tailed Wilcoxon test.

357 For the comparison of viability between strains during log-phase growth at 39°C in Figure 3A, strains were
358 streaked out and three colonies of each were pre-cultured at 28°C, back-diluted, and cultured at 39°C, as for
359 the 39°C growth assays above. After 24 hours of incubation at 39°C, for each such replicate culture, spotting of
360 dilutions and colony counting to yield CFU/mL/OD₆₀₀ for each replicate liquid culture was done as above,
361 except that we used two technical replicate spotting assay replicates for each culture, taking the average
362 across them as the final report of viability. The vector of these viability measurements across replicates for a
363 given strain was compared to that from *S. paradoxus* with a one-tailed Wilcoxon test.

364 For the comparison of viability between strains in stationary phase at 39°C in Figure 3B, strains were streaked
365 out and three colonies of each were pre-cultured at 28°C as for the 39°C growth assays above, except that
366 that the initial pre-culture to achieve saturation lasted 72 hours. Each such replicate culture was then incubated
367 (without back-dilution) at 39°C for 24 hours, after which spotting, colony counting, and statistical testing were
368 as for Figure 3A.

369 For the comparison of viability between strains during log-phase growth at 28°C in Figure S5A, strains were
370 streaked out and four colonies of each were pre-cultured at 28°C and back-diluted as for the 39°C growth
371 assays above; each back-diluted replicate culture was incubated at 28°C for 24 hours, after which spotting and
372 colony counting was as above. For the comparison of viability between strains in stationary phase at 28°C in
373 Figure S5B, strains were streaked out as above, and three colonies of each were inoculated into liquid YPD at
374 28°C and incubated for 96 hours, after which spotting, colony counting, and statistical testing were as for
375 Figure 3A, except that a two-sided Wilcoxon tests were performed.

376 For the comparison of viability between environmental strains during log-phase growth at 4°C (Figure S6),
377 aliquots from cultures set up for cold growth assays (see above) were taken at day 8 of the cold timecourse for
378 spotting, colony counting, and statistical testing as for Figure 3A.

379 **Epistasis analysis**

380 For Figure 2A, we calculated the growth phenotype at 39°C of the strain harboring all eight *S. cerevisiae* loci in
381 the *S. paradoxus* background as expected under a model of independent locus effects as follows. We first
382 tabulated the mean growth efficiency at 39°C of each isogenic strain in turn with just one gene swapped in
383 from *S. cerevisiae* and the analogous mean for *S. paradoxus*, and took the difference between them,
384 representing the mean effect of the respective swap; we then summed the latter effect values across all eight
385 loci. Error bars were calculated by bootstrapping as follows. For each locus, we generated a random sample of
386 the replicate measurements of the growth efficiency of the respective swap strain at 39°C with replacement,
387 and took the mean; we calculated an analogous mean from a random sample of replicates of the *S. paradoxus*
388 wild-type; and we took the difference between these means, representing one bootstrapped estimate of the
389 effect of the swap. We then took the sum of such effects across all loci, representing one bootstrap's worth of
390 the estimate of the eight-gene transgenic's phenotype under the additive model. We repeated this procedure
391 10,000 times to set up a distribution of the estimated sum, and we identified the values corresponding to the
392 68% confidence interval.

393 For a given panel of Figure 2B, the left-hand point on the plot reports the mean effect of the *S. cerevisiae* allele
394 of the respective gene when swapped alone into *S. paradoxus*. For this we tabulated the mean growth
395 efficiency at 39°C of this single-gene transgenic across all replicates and the analogous mean across all
396 replicates of *S. paradoxus*, and took the difference between them. For the error bar, we generated a random
397 sample of the replicate measurements of the growth efficiency of the respective swap strain at 39°C with
398 replacement, and took the mean; we calculated an analogous mean from a random sample of replicates of the
399 *S. paradoxus* wild-type; and we took the difference between these means, representing one bootstrapped
400 estimate of the effect of the swap. We repeated this procedure 10,000 times to set up a distribution of the
401 effect value, and we identified the values corresponding to the 68% confidence interval. The right-hand point
402 on the plot reports the mean effect of the *S. cerevisiae* allele of the respective gene when swapped into a
403 multi-genic strain of the *S. paradoxus* background in the series culminating in the eight-fold transgenic, in the
404 order of Figure 1; call the strain before and after the replacement of the gene of interest *X-1* and *X*,

405 respectively. We tabulated the mean growth efficiency at 39°C across all replicates of strain *X* and the
406 analogous quantity for strain *X-1*, and took the difference between them. Error bars were calculated by
407 bootstrapping as above.

408

409

410

Gene	GO terms	Location	Description	Protein Length (residues)	Protein Identity (%)
<i>AFG2/YLR397C</i>	ribosomal large subunit biogenesis	Ch. XII 912550 - 914892	Essential for pre-60S maturation and release of several pre-ribosome maturation factors	780	93.6
<i>APC1/YNL172W</i>	mitotic cell cycle	Ch. XIV 310636 - 315882	Largest subunit of the Anaphase-Promoting Complex; a ubiquitin-protein ligase required for degradation of anaphase inhibitors	1748	90.6
<i>CEP3/YMR168C</i>	mitotic cell cycle	Ch. XIII 597332 - 599158	Essential kinetochore protein; component of the CBF3 complex that binds the CDEIII region of the centromere	575	93.2
<i>DYN1/YKR054C</i>	mitotic cell cycle	Ch. XI 535647 - 547925	Heavy chain dynein; microtubule motor protein; required for anaphase spindle elongation	4092	87.5
<i>ESP1/YGR098C</i>	mitotic cell cycle	Ch. VII 682566 - 687458	Separase/separin; aids in the dislocation of cohesin from chromatin and sister chromatin segregation.	1630	89.9
<i>MYO1/YHR023W</i>	mitotic cell cycle	Ch. VIII 151666 - 157452	Type II myosin heavy chain; required for cytokinesis and cell separation	1928	91.9
<i>SCC2/YDR180W</i>	mitotic cell cycle	Ch. IV 821295 - 825776	A complex required for loading of cohesin complexes onto chromosomes; involved in establishing sister chromatid cohesion during DSB repair via histone H2AX; subunit of cohesin loading factor (SCC2p-Scc4p)	1493	88.2

<i>TAF2/YCR042C</i>	chromatin binding	Ch. III 201174 - 205397	TFIID subunit; involved in RNA polymerase II transcription initiation	1407	89.8
---------------------	----------------------	----------------------------	--	------	------

411 **Table 1. Genes contributing to thermotolerance divergence between *Saccharomyces cerevisiae* and *S.***
412 ***paradoxus*.** GO, Gene Ontology biological process. The last column reports amino acid divergence between
413 *S. cerevisiae* DBVPG1373 and *S. paradoxus* Z1.
414
415

416

417 References

- 418 1. Linnen CR, Poh Y-P, Peterson BK, Barrett RDH, Larson JG, Jensen JD, et al. Adaptive evolution
419 of multiple traits through multiple mutations at a single gene. *Science*. 2013;339: 1312–1316.
420 doi:10.1126/science.1233213
- 421 2. Chan YF, Marks ME, Jones FC, Villarreal G, Shapiro MD, Brady SD, et al. Adaptive evolution of
422 pelvic reduction in sticklebacks by recurrent deletion of a Pitx1 enhancer. *Science*. 2010;327:
423 302–305. doi:10.1126/science.1182213
- 424 3. Weber K, Eisman R, Morey L, Patty A, Sparks J, Tausek M, et al. An analysis of polygenes
425 affecting wing shape on chromosome 3 in *Drosophila melanogaster*. *Genetics*. 1999;153: 773–
426 786.
- 427 4. Bridgham JT, Ortlund EA, Thornton JW. An epistatic ratchet constrains the direction of
428 glucocorticoid receptor evolution. *Nature*. 2009;461: 515–519. doi:10.1038/nature08249
- 429 5. Boyle EA, Li YI, Pritchard JK. An Expanded View of Complex Traits: From Polygenic to
430 Omnigenic. *Cell*. 2017;169: 1177–1186. doi:10.1016/j.cell.2017.05.038
- 431 6. Castro JP, Yancoskie MN, Marchini M, Belohlavy S, Hiramatsu L, Kučka M, et al. An integrative
432 genomic analysis of the Longshanks selection experiment for longer limbs in mice. *Elife*. 2019;8.
433 doi:10.7554/eLife.42014
- 434 7. Liu Q, Onal P, Datta RR, Rogers JM, Schmidt-Ott U, Bulyk ML, et al. Ancient mechanisms for
435 the evolution of the bicoid homeodomain's function in fly development. *Elife*. 2018;7.
436 doi:10.7554/eLife.34594
- 437 8. Aggeli D, Li Y, Sherlock G. Changes in the distribution of fitness effects and adaptive mutational
438 spectra following a single first step towards adaptation. *Evolutionary Biology*; 2020 Jun.
439 doi:10.1101/2020.06.12.148833
- 440 9. Shen JP, Zhao D, Sasik R, Luebeck J, Birmingham A, Bojorquez-Gomez A, et al. Combinatorial
441 CRISPR-Cas9 screens for de novo mapping of genetic interactions. *Nat Methods*. 2017;14: 573–
442 576. doi:10.1038/nmeth.4225
- 443 10. Neverov AD, Kryazhimskiy S, Plotkin JB, Bazykin GA. Coordinated Evolution of Influenza A
444 Surface Proteins. *PLoS Genet*. 2015;11: e1005404. doi:10.1371/journal.pgen.1005404
- 445 11. Weinreich DM, Delaney NF, Depristo MA, Hartl DL. Darwinian evolution can follow only very few
446 mutational paths to fitter proteins. *Science*. 2006;312: 111–114. doi:10.1126/science.1123539
- 447 12. Wong ASL, Choi GCG, Lu TK. Deciphering Combinatorial Genetics. *Annu Rev Genet*. 2016;50:
448 515–538. doi:10.1146/annurev-genet-120215-034902
- 449 13. Palmer AC, Toprak E, Baym M, Kim S, Veres A, Bershtein S, et al. Delayed commitment to
450 evolutionary fate in antibiotic resistance fitness landscapes. *Nat Commun*. 2015;6: 7385.
451 doi:10.1038/ncomms8385

- 452 14. Fisher KJ, Kryazhimskiy S, Lang GI. Detecting genetic interactions using parallel evolution in
453 experimental populations. *Philos Trans R Soc Lond B Biol Sci*. 2019;374: 20180237.
454 doi:10.1098/rstb.2018.0237
- 455 15. Csilléry K, Rodríguez-Verdugo A, Rellstab C, Guillaume F. Detecting the genomic signal of
456 polygenic adaptation and the role of epistasis in evolution. *Mol Ecol*. 2018;27: 606–612.
457 doi:10.1111/mec.14499
- 458 16. Chou H-H, Chiu H-C, Delaney NF, Segrè D, Marx CJ. Diminishing returns epistasis among
459 beneficial mutations decelerates adaptation. *Science*. 2011;332: 1190–1192.
460 doi:10.1126/science.1203799
- 461 17. Weiss CV, Brem RB. Dissecting Trait Variation across Species Barriers. *Trends Ecol Evol*.
462 2019;34: 1131–1136. doi:10.1016/j.tree.2019.07.013
- 463 18. Xie KT, Wang G, Thompson AC, Wucherpfennig JI, Reimchen TE, MacColl ADC, et al. DNA
464 fragility in the parallel evolution of pelvic reduction in stickleback fish. *Science*. 2019;363: 81–84.
465 doi:10.1126/science.aan1425
- 466 19. Savolainen O, Lascoux M, Merilä J. Ecological genomics of local adaptation. *Nat Rev Genet*.
467 2013;14: 807–820. doi:10.1038/nrg3522
- 468 20. Okada Y. Effects of isoproterenol on chemical carcinogenesis with DMBA in mouse salivary
469 glands. *J Oral Pathol*. 1979;8: 340–350. doi:10.1111/j.1600-0714.1979.tb01837.x
- 470 21. Lofgren DL, Stewart TS. Efficacy of alternative multivariate best linear unbiased prediction
471 models for genetic evaluation of swine. *J Anim Sci*. 1991;69: 4388–4396.
472 doi:10.2527/1991.69114388x
- 473 22. Mackay TFC. Epistasis and quantitative traits: using model organisms to study gene-gene
474 interactions. *Nat Rev Genet*. 2014;15: 22–33. doi:10.1038/nrg3627
- 475 23. Starr TN, Thornton JW. Epistasis in protein evolution. *Protein Sci*. 2016;25: 1204–1218.
476 doi:10.1002/pro.2897
- 477 24. Gonçalves P, Valério E, Correia C, de Almeida JMGCF, Sampaio JP. Evidence for divergent
478 evolution of growth temperature preference in sympatric *Saccharomyces* species. *PLoS One*.
479 2011;6: e20739. doi:10.1371/journal.pone.0020739
- 480 25. Anderson DP, Whitney DS, Hanson-Smith V, Woznica A, Campodonico-Burnett W, Volkman BF,
481 et al. Evolution of an ancient protein function involved in organized multicellularity in animals.
482 *Elife*. 2016;5: e10147. doi:10.7554/eLife.10147
- 483 26. Williams KM, Liu P, Fay JC. Evolution of ecological dominance of yeast species in high-sugar
484 environments. *Evolution*. 2015;69: 2079–2093. doi:10.1111/evo.12707
- 485 27. Finnigan GC, Hanson-Smith V, Stevens TH, Thornton JW. Evolution of increased complexity in a
486 molecular machine. *Nature*. 2012;481: 360–364. doi:10.1038/nature10724
- 487 28. Toprak E, Veres A, Michel J-B, Chait R, Hartl DL, Kishony R. Evolutionary paths to antibiotic
488 resistance under dynamically sustained drug selection. *Nat Genet*. 2011;44: 101–105.

- 489 doi:10.1038/ng.1034
- 490 29. Lindsey HA, Gallie J, Taylor S, Kerr B. Evolutionary rescue from extinction is contingent on a
491 lower rate of environmental change. *Nature*. 2013;494: 463–467. doi:10.1038/nature11879
- 492 30. Burke MK, Rose MR. Experimental evolution with *Drosophila*. *Am J Physiol Regul Integr Comp*
493 *Physiol*. 2009;296: R1847-1854. doi:10.1152/ajpregu.90551.2008
- 494 31. Ritchie MD. Finding the epistasis needles in the genome-wide haystack. *Methods Mol Biol*.
495 2015;1253: 19–33. doi:10.1007/978-1-4939-2155-3_2
- 496 32. Weiss CV, Roop JI, Hackley RK, Chuong JN, Grigoriev IV, Arkin AP, et al. Genetic dissection of
497 interspecific differences in yeast thermotolerance. *Nat Genet*. 2018;50: 1501–1504.
498 doi:10.1038/s41588-018-0243-4
- 499 33. Baryshnikova A, Costanzo M, Myers CL, Andrews B, Boone C. Genetic interaction networks:
500 toward an understanding of heritability. *Annu Rev Genomics Hum Genet*. 2013;14: 111–133.
501 doi:10.1146/annurev-genom-082509-141730
- 502 34. Peter J, De Chiara M, Friedrich A, Yue J-X, Pflieger D, Bergström A, et al. Genome evolution
503 across 1,011 *Saccharomyces cerevisiae* isolates. *Nature*. 2018;556: 339–344.
504 doi:10.1038/s41586-018-0030-5
- 505 35. Blount ZD, Barrick JE, Davidson CJ, Lenski RE. Genomic analysis of a key innovation in an
506 experimental *Escherichia coli* population. *Nature*. 2012;489: 513–518. doi:10.1038/nature11514
- 507 36. Herbst RH, Bar-Zvi D, Reikhav S, Soifer I, Breker M, Jona G, et al. Heterosis as a consequence
508 of regulatory incompatibility. *BMC Biol*. 2017;15: 38. doi:10.1186/s12915-017-0373-7
- 509 37. Johnson MS, Martsul A, Kryazhimskiy S, Desai MM. Higher-fitness yeast genotypes are less
510 robust to deleterious mutations. *Science*. 2019;366: 490–493. doi:10.1126/science.aay4199
- 511 38. Buskirk SW, Peace RE, Lang GI. Hitchhiking and epistasis give rise to cohort dynamics in
512 adapting populations. *Proc Natl Acad Sci U S A*. 2017;114: 8330–8335.
513 doi:10.1073/pnas.1702314114
- 514 39. Will JL, Kim HS, Clarke J, Painter JC, Fay JC, Gasch AP. Incipient balancing selection through
515 adaptive loss of aquaporins in natural *Saccharomyces cerevisiae* populations. *PLoS Genet*.
516 2010;6: e1000893. doi:10.1371/journal.pgen.1000893
- 517 40. Marcusson LL, Frimodt-Møller N, Hughes D. Interplay in the selection of fluoroquinolone
518 resistance and bacterial fitness. *PLoS Pathog*. 2009;5: e1000541.
519 doi:10.1371/journal.ppat.1000541
- 520 41. Wisner MJ, Ribbeck N, Lenski RE. Long-term dynamics of adaptation in asexual populations.
521 *Science*. 2013;342: 1364–1367. doi:10.1126/science.1243357
- 522 42. Bons E, Leemann C, Metzner KJ, Regoes RR. Long-term experimental evolution of HIV-1
523 reveals effects of environment and mutational history. *PLoS Biol*. 2020;18: e3001010.
524 doi:10.1371/journal.pbio.3001010

- 525 43. Tutuncuoglu B, Krogan NJ. Mapping genetic interactions in cancer: a road to rational
526 combination therapies. *Genome Med.* 2019;11: 62. doi:10.1186/s13073-019-0680-4
- 527 44. Kryazhimskiy S, Rice DP, Jerison ER, Desai MM. Microbial evolution. Global epistasis makes
528 adaptation predictable despite sequence-level stochasticity. *Science.* 2014;344: 1519–1522.
529 doi:10.1126/science.1250939
- 530 45. Li XC, Peris D, Hittinger CT, Sia EA, Fay JC. Mitochondria-encoded genes contribute to
531 evolution of heat and cold tolerance in yeast. *Sci Adv.* 2019;5: eaav1848.
532 doi:10.1126/sciadv.aav1848
- 533 46. Baker EP, Peris D, Moriarty RV, Li XC, Fay JC, Hittinger CT. Mitochondrial DNA and
534 temperature tolerance in lager yeasts. *Sci Adv.* 2019;5: eaav1869. doi:10.1126/sciadv.aav1869
- 535 47. Wolters JF, Charron G, Gaspary A, Landry CR, Fiumera AC, Fiumera HL. Mitochondrial
536 Recombination Reveals Mito-Mito Epistasis in Yeast. *Genetics.* 2018;209: 307–319.
537 doi:10.1534/genetics.117.300660
- 538 48. Iranmehr A, Stobdan T, Zhou D, Zhao H, Kryazhimskiy S, Bafna V, et al. Multiple mechanisms
539 drive genomic adaptation to extreme O₂ levels in *Drosophila melanogaster*. *Nat Commun.*
540 2021;12: 997. doi:10.1038/s41467-021-21281-6
- 541 49. Khan AI, Dinh DM, Schneider D, Lenski RE, Cooper TF. Negative epistasis between beneficial
542 mutations in an evolving bacterial population. *Science.* 2011;332: 1193–1196.
543 doi:10.1126/science.1203801
- 544 50. Linnen CR, Kingsley EP, Jensen JD, Hoekstra HE. On the origin and spread of an adaptive
545 allele in deer mice. *Science.* 2009;325: 1095–1098. doi:10.1126/science.1175826
- 546 51. Avery L, Wasserman S. Ordering gene function: the interpretation of epistasis in regulatory
547 hierarchies. *Trends Genet.* 1992;8: 312–316. doi:10.1016/0168-9525(92)90263-4
- 548 52. Pillai AS, Chandler SA, Liu Y, Signore AV, Cortez-Romero CR, Benesch JLP, et al. Origin of
549 complexity in haemoglobin evolution. *Nature.* 2020;581: 480–485. doi:10.1038/s41586-020-
550 2292-y
- 551 53. Weinreich DM, Watson RA, Chao L. Perspective: Sign epistasis and genetic constraint on
552 evolutionary trajectories. *Evolution.* 2005;59: 1165–1174.
- 553 54. Johnson MS, Gopalakrishnan S, Goyal J, Dillingham ME, Bakerlee CW, Humphrey PT, et al.
554 Phenotypic and molecular evolution across 10,000 generations in laboratory budding yeast
555 populations. *eLife.* 2021;10: e63910. doi:10.7554/eLife.63910
- 556 55. Hewitt SK, Duangrattanaalert K, Burgis T, Zeef LAH, Naseeb S, Delneri D. Plasticity of
557 Mitochondrial DNA Inheritance and its Impact on Nuclear Gene Transcription in Yeast Hybrids.
558 *Microorganisms.* 2020;8. doi:10.3390/microorganisms8040494
- 559 56. Roop JI, Chang KC, Brem RB. Polygenic evolution of a sugar specialization trade-off in yeast.
560 *Nature.* 2016;530: 336–339. doi:10.1038/nature16938
- 561 57. Abrams MB, Dubin CA, AlZaben F, Bravo J, Joubert PM, Weiss CV, et al. Population and

- 562 comparative genetics of thermotolerance divergence between yeast species. Gresham D, editor.
563 G3 Genes|Genomes|Genetics. 2021; jkab139. doi:10.1093/g3journal/jkab139
- 564 58. Liti G, Carter DM, Moses AM, Warringer J, Parts L, James SA, et al. Population genomics of
565 domestic and wild yeasts. *Nature*. 2009;458: 337–341. doi:10.1038/nature07743
- 566 59. Messer PW, Petrov DA. Population genomics of rapid adaptation by soft selective sweeps.
567 *Trends Ecol Evol*. 2013;28: 659–669. doi:10.1016/j.tree.2013.08.003
- 568 60. Špírek M, Poláková S, Jatzová K, Sulo P. Post-zygotic sterility and cytonuclear compatibility
569 limits in *S. cerevisiae* xenomitochondrial cybrids. *Front Genet*. 2014;5: 454.
570 doi:10.3389/fgene.2014.00454
- 571 61. Gusareva ES, Van Steen K. Practical aspects of genome-wide association interaction analysis.
572 *Hum Genet*. 2014;133: 1343–1358. doi:10.1007/s00439-014-1480-y
- 573 62. Escudero JA, Nivina A, Kemble HE, Loot C, Tenaillon O, Mazel D. Primary and promiscuous
574 functions coexist during evolutionary innovation through whole protein domain acquisitions. *Elife*.
575 2020;9. doi:10.7554/eLife.58061
- 576 63. Roth FP, Lipshitz HD, Andrews BJ. Q&A: epistasis. *J Biol*. 2009;8: 35. doi:10.1186/jbiol144
- 577 64. Goddard MR. Quantifying the complexities of *Saccharomyces cerevisiae*'s ecosystem
578 engineering via fermentation. *Ecology*. 2008;89: 2077–2082. doi:10.1890/07-2060.1
- 579 65. Hittinger CT. *Saccharomyces* diversity and evolution: a budding model genus. *Trends Genet*.
580 2013;29: 309–317. doi:10.1016/j.tig.2013.01.002
- 581 66. Lynch M. Scaling expectations for the time to establishment of complex adaptations. *Proc Natl*
582 *Acad Sci U S A*. 2010;107: 16577–16582. doi:10.1073/pnas.1010836107
- 583 67. Sweeney JY, Kuehne HA, Sniegowski PD. Sympatric natural *Saccharomyces cerevisiae* and *S.*
584 *paradoxus* populations have different thermal growth profiles. *FEMS Yeast Res*. 2004;4: 521–
585 525. doi:10.1016/S1567-1356(03)00171-5
- 586 68. Salvadó Z, Arroyo-López FN, Guillamón JM, Salazar G, Querol A, Barrio E. Temperature
587 adaptation markedly determines evolution within the genus *Saccharomyces*. *Appl Environ*
588 *Microbiol*. 2011;77: 2292–2302. doi:10.1128/AEM.01861-10
- 589 69. Good BH, McDonald MJ, Barrick JE, Lenski RE, Desai MM. The dynamics of molecular evolution
590 over 60,000 generations. *Nature*. 2017;551: 45–50. doi:10.1038/nature24287
- 591 70. Hong W, Takshak A, Osunbayo O, Kunwar A, Vershinin M. The Effect of Temperature on
592 Microtubule-Based Transport by Cytoplasmic Dynein and Kinesin-1 Motors. *Biophys J*.
593 2016;111: 1287–1294. doi:10.1016/j.bpj.2016.08.006
- 594 71. Orteu A, Jiggins CD. The genomics of coloration provides insights into adaptive evolution. *Nat*
595 *Rev Genet*. 2020;21: 461–475. doi:10.1038/s41576-020-0234-z
- 596 72. Hoekstra HE, Coyne JA. The locus of evolution: evo devo and the genetics of adaptation.
597 *Evolution*. 2007;61: 995–1016. doi:10.1111/j.1558-5646.2007.00105.x

- 598 73. Tenailon O, Rodríguez-Verdugo A, Gaut RL, McDonald P, Bennett AF, Long AD, et al. The
599 molecular diversity of adaptive convergence. *Science*. 2012;335: 457–461.
600 doi:10.1126/science.1212986
- 601 74. Sella G, Barton NH. Thinking About the Evolution of Complex Traits in the Era of Genome-Wide
602 Association Studies. *Annu Rev Genomics Hum Genet*. 2019;20: 461–493. doi:10.1146/annurev-
603 genom-083115-022316
- 604 75. Pardo-Diaz C, Salazar C, Jiggins CD. Towards the identification of the loci of adaptive evolution.
605 *Methods Ecol Evol*. 2015;6: 445–464. doi:10.1111/2041-210X.12324
- 606

607 Figure captions

608 **Figure 1. *S. cerevisiae* alleles of thermotolerance loci jointly improve growth at high temperature.** In
609 each plot, the y-axis reports growth efficiency at 39°C, the cell density after a 24-hour incubation as a
610 difference from the starting density. In the main plot, each column reports data from a transgenic *S. paradoxus*
611 strain harboring *S. cerevisiae* alleles of the indicated thermotolerance loci, or the wild-type *S. paradoxus*
612 progenitor. At bottom, each cell reports the genotype at the indicated locus in the indicated strain. The inset
613 shows purebred wild-types and the *S. paradoxus* strain harboring all eight thermotolerance loci from *S.*
614 *cerevisiae* (8x swap); the y-axis is log-scaled. Black points report individual biological replicates and white dots
615 report means. Boxes span the interquartile range. Whiskers are 1.5 times the interquartile range. Statistical
616 analyses are reported in Table S1A.

617 **Figure 2. Negative epistasis among *S. cerevisiae* alleles of thermotolerance loci.** (A) Solid bars report
618 growth efficiency at 39°C for purebred *S. paradoxus* and the *S. paradoxus* strain harboring all eight
619 thermotolerance loci from *S. cerevisiae* (8x swap). In the right column, the hollow extension reports the sum of
620 the efficiencies at 39°C of *S. paradoxus* strains harboring individual thermotolerance loci from *S. cerevisiae*,
621 from Figure S3. (B) In a given panel, the right-hand point shows the effect, on efficiency at 39°C, of the *S.*
622 *cerevisiae* allele of the indicated gene when introduced into a transgenic also harboring *S. cerevisiae* alleles of
623 other genes, in the series of **Figure 1**. The left-hand point shows the analogous quantity when wild-type *S.*
624 *paradoxus* was the background. Error bars report 68% confidence intervals.

625 **Figure 3. *S. cerevisiae* alleles of thermotolerance loci jointly improve heat survival during growth but**
626 **not in stationary phase.** In a given panel, each column reports viability after heat treatment of the wild-type of
627 the indicated species, or the *S. paradoxus* strain harboring eight thermotolerance loci from *S. cerevisiae* (8x
628 swap). The y-axis reports the number of colonies formed on solid medium from 1 mL of heat-treated liquid
629 culture in (A) logarithmic growth or (B) stationary phase, normalized by turbidity. Points and bar heights report
630 individual biological replicates and their means, respectively. *, Wilcoxon $p \leq 0.05$.

631 **Figure 4. *S. cerevisiae* alleles of thermotolerance loci jointly compromise growth in the cold.** (A) Each
632 trace reports a timecourse of growth at 4°C of the wild-type of the indicated species, or the *S. paradoxus* strain
633 harboring eight thermotolerance loci from *S. cerevisiae* (8x swap). For a given strain, points on a given day
634 report biological replicates; lines report the average fit from a logistic regression across replicates (Table S2).
635 (B) The y-axis reports growth rate, in units of cell density (optical density, OD) per day, from the average
636 logistic fit of the timecourse in (A) for the indicated strain. (C) The y-axis reports, for day 10 of the timecourse in
637 (A) for the indicated strain, growth efficiency, the cell density after a 10-day incubation at 4°C as a difference
638 from the starting density. In (B) and (C), points report individual biological replicates. Boxes show the median
639 and span the interquartile range of the data (IQR, 25%-75%); whiskers are 1.5 times the interquartile range,
640 and do not report outliers. ** and ***, Wilcoxon $p \leq 0.004$ and $p \leq 0.0005$, respectively.

641

642 Supplementary table captions

643
644 **Table S1. Statistical analyses of growth at 39°C and 28°C.** (A) Each cell reports the results of a one-sided
645 Wilcoxon test comparing growth efficiency at 39°C between the indicated strains, in Figure 1 of the main text.
646 Multiple testing was corrected for using the Benjamini-Hochberg method. (B) Data are as in A except that
647 analysis was of growth efficiency at 28°C from Figure S1 and two-sided Wilcoxon tests were applied.

648 **Table S2. Parameters used in regressions.** Each row reports fitted values of the indicated parameters from
649 the polynomial regression (Figure S2) or logistic regression (all other figures) of growth measurements of the
650 indicated strain for the indicated figure. For the logistic regression, K, R, and x_0 are the carrying capacity,
651 logistic growth rate, and the sigmoidal midpoint, respectively.

652 **Table S3. Strains used in this study. A.** Wild-type diploid strains, including those used as parents of allele-
653 replacement transgenesis; SGRP, the Saccharomyces Genome Resequencing Project, version 2. **B.** Allele
654 replacement strains in *S. paradoxus* Z1 diploid homozygote backgrounds. In genotype notes, e.g., in an *S.*
655 *paradoxus* background, $\Delta YFG(-X \text{ to } +Y)::scYFG(-Z \text{ to } +W)$ indicates that in *S. paradoxus* Z1, bases -X to +Y
656 from gene YFG have been removed and replaced by bases -Z to +W of the allele of YFG from the indicated *S.*
657 *cerevisiae* strain. Positive coordinates count in the 5' to 3' direction from the start codon (+1 corresponds to the
658 A in the ATG), and negative coordinates count in the 3' to 5' direction from the start codon (-1 corresponds to
659 the base directly 5' of the ATG). In cases where the replacement extended into a region of 100% conservation
660 between species, the position of the last divergent nucleotide is shown.

661

662 Supplementary figure captions

663 **Figure S1. Allelic variation at thermotolerance loci has little growth impact at 28°C.** Data and symbols
664 are as in Figure 1 of the main text except that growth was measured at 28°C. Statistical analyses are reported
665 in Table S1B.

666 **Figure S2. *S. cerevisiae* alleles of thermotolerance loci jointly improve growth at temperatures from**
667 **37°C - 39°C.** In a given panel, each trace reports growth efficiency, the cell density after a 24-hour incubation
668 at the indicated temperature as a difference from the starting density, of the wild-type of the indicated species
669 or the *S. paradoxus* strain harboring eight thermotolerance loci from *S. cerevisiae* (8x swap). Lines are the
670 result of a polynomial regression on the points (Table S2). *, Wilcoxon $p \leq 0.0404$.

671 **Figure S3. *S. cerevisiae* alleles of thermotolerance loci individually improve growth at high**
672 **temperature.** Data and symbols are as in the main panel of Figure 1 except that each column reports results
673 from the indicated wild-type strain or a strain of *S. paradoxus* harboring the *S. cerevisiae* allele of the indicated
674 single gene and the y -axis is log-scaled. All comparisons to *S. paradoxus* had one-sided Wilcoxon $p < 0.01$
675 after correction for multiple testing.

676 **Figure S4. Environmental isolates of *Saccharomyces* spp. differ in heat survival.** Each cell reports
677 viability after heat treatment of the indicated strain and species. Each cell reports the number of colonies
678 formed on solid medium from 1 mL of heat-treated liquid culture in logarithmic growth, normalized by the
679 turbidity of the latter. *S. paradoxus* Z1, N17, and A12 are isolates from UK, Russia, and Quebec, respectively;
680 *S. cerevisiae* strains DBVPG1373, DBVPG1788, YPS128 are from the Netherlands, Finland, and
681 Pennsylvania, respectively. Viability was different between species at Wilcoxon $p < 0.00002$ for all
682 temperatures.

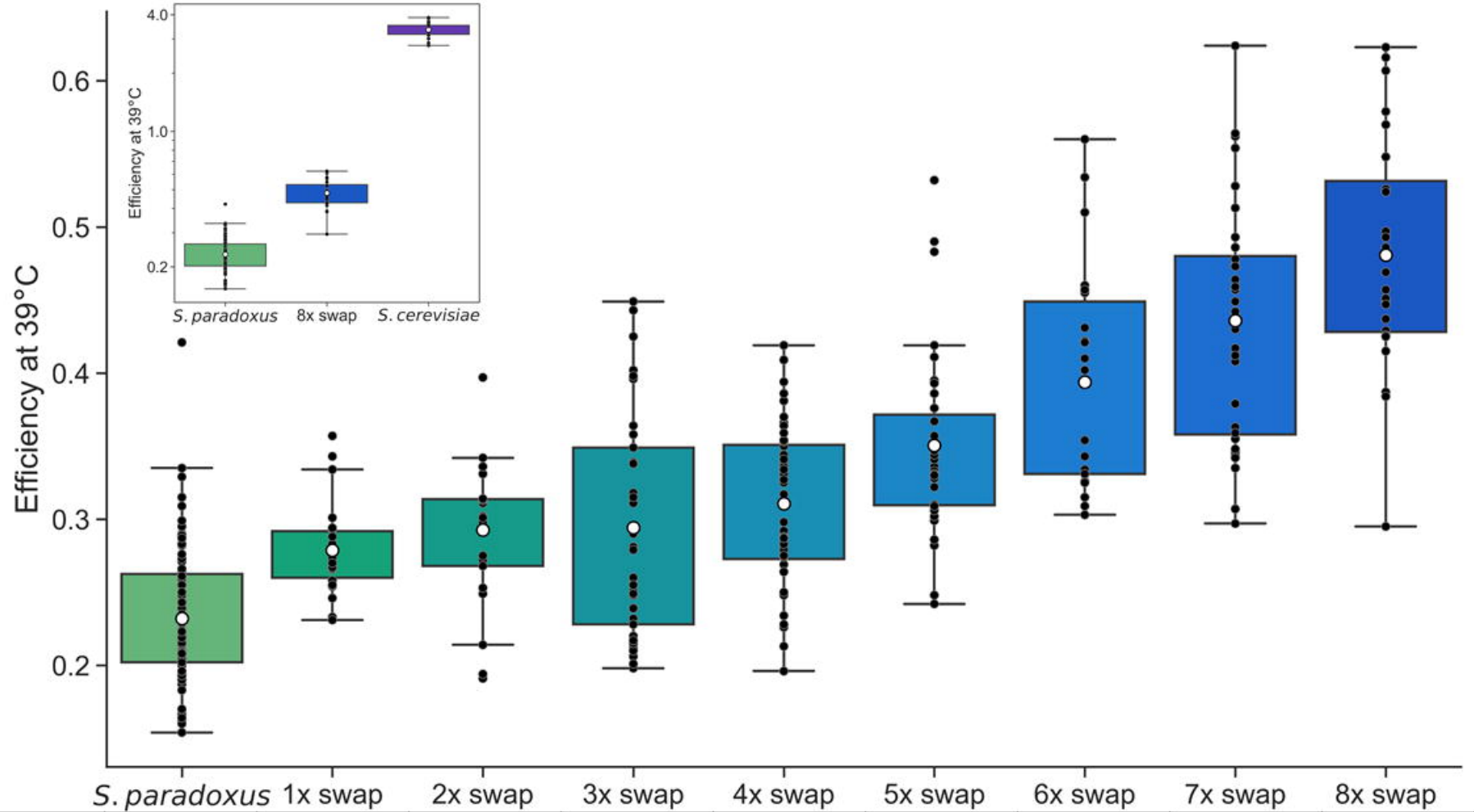
683 **Figure S5. Allelic variation at thermotolerance loci has no impact on viability at 28°C.** Data and symbols
684 are as in Figure 3 of the main text except that liquid incubations were at 28°C. In no case was the respective
685 measurement for a given strain significantly different from the analogous quantity for *S. paradoxus* at two-sided
686 Wilcoxon $p < 0.05$.

687 **Figure S6. Environmental isolates of *Saccharomyces* spp. differ in ability to grow at 4°C.** (A) Each trace
688 reports a timecourse of growth at 4°C of the wild-type of the indicated strain. For a given strain, points on a
689 given day report biological replicates; lines report the average fit from a logistic regression across replicates
690 (Table S2). YPS128, a North American *S. cerevisiae* known to have recently acquired freeze-thaw resistance
691 as a derived character distinct from the ancestral program (Will et al., 2010), is shown in faint blue. (B) The y-
692 axis reports growth rate, in units of cell density (optical density, OD) per day, from the average logistic fit of the
693 timecourse in (A) for the indicated strain. (C) The y-axis reports, for day 10 of the timecourse in (A) for the
694 indicated strain, growth efficiency, the cell density after a 10-day incubation at 4°C as a difference from the
695 starting density. In (B) and (C), Black points report individual biological replicates. White dots report means.
696 Boxes span the interquartile range; whiskers are 1.5 times the interquartile range, and do not report outliers.
697 Comparisons of growth rate and efficiency at 4°C between *S. paradoxus* strains and *S. cerevisiae* strains
698 yielded Wilcoxon $p \leq 0.00003$ and $p \leq 0.002$, respectively.

699 **Figure S7. Growth effects at 4°C of *S. cerevisiae* alleles of individual thermotolerance loci.** (A) Data and
700 symbols are as in Figure S3 except that the y-axis reports growth efficiency after a 10-day incubation at 4°C.
701 (B) Data are as in (A) except that the y-axis reports growth rate, in units of cell density (optical density, OD) per
702 day, from the average logistic fit of the timecourse for the indicated strain (Table S2). * and **, one-sided
703 Wilcoxon $p \leq 0.05$ and 0.01 , respectively.

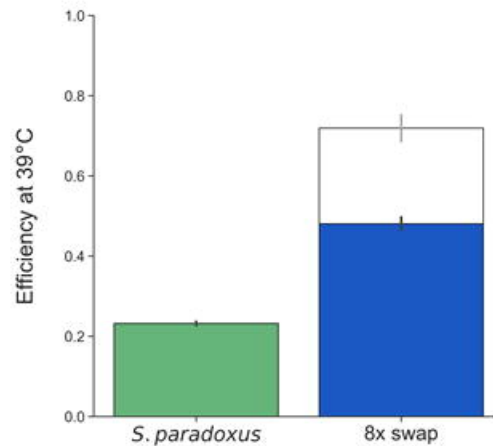
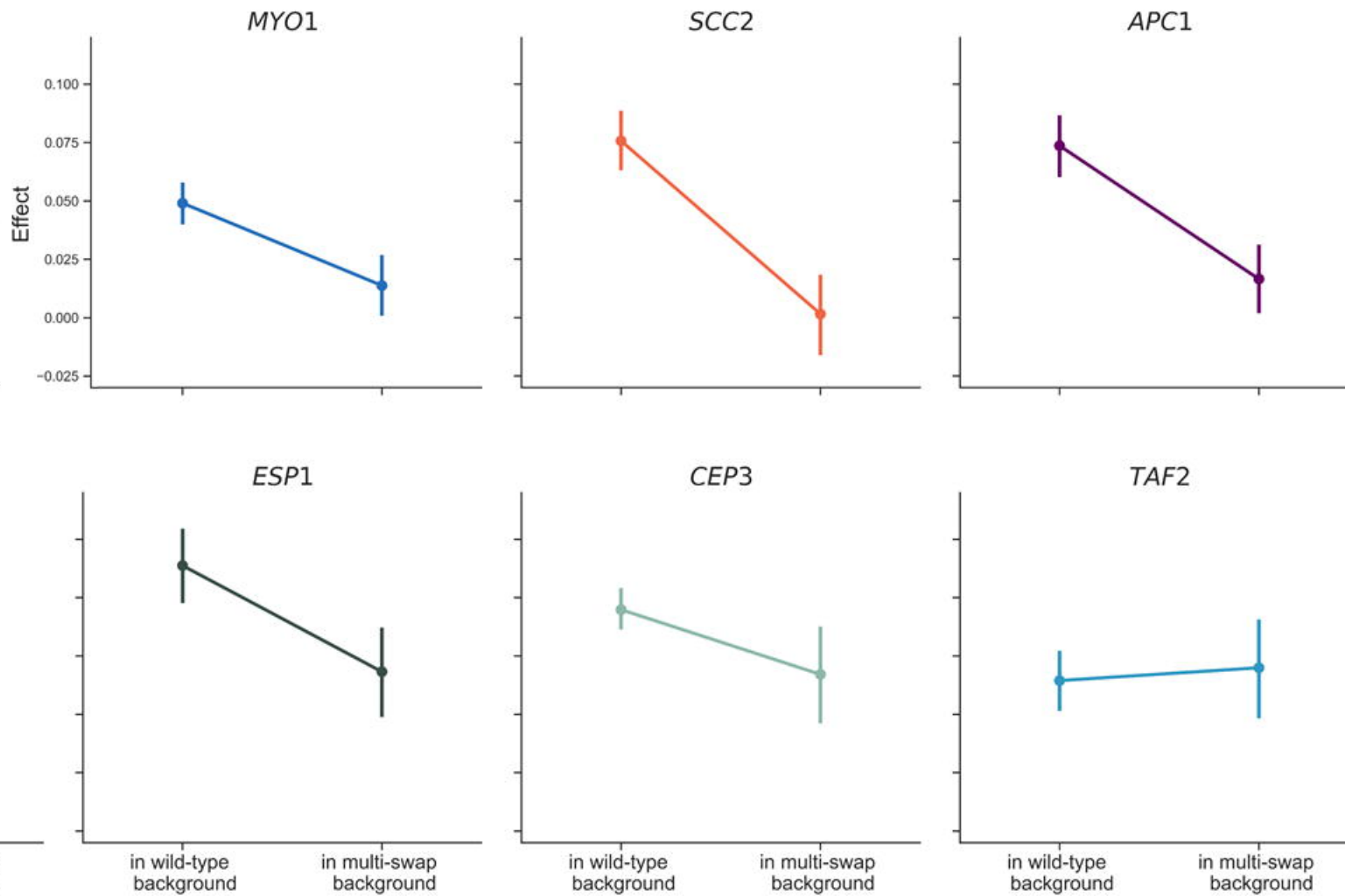
704 **Figure S8. Joint growth effects at 4°C of *S. cerevisiae* alleles of subsets of thermotolerance loci.** (A)
705 Data and symbols are as in the main panel of Figure 1 except that the y-axis reports growth efficiency after a
706 10-day incubation at 4°C. (B) Data and symbols are as in (A) except that the y-axis reports growth rate, in units
707 of cell density (optical density, OD) per day, from the average logistic fit of the timecourse for the indicated
708 strain (Table S2). * and **, one-sided Wilcoxon $p \leq 0.05$ and 0.01 respectively.

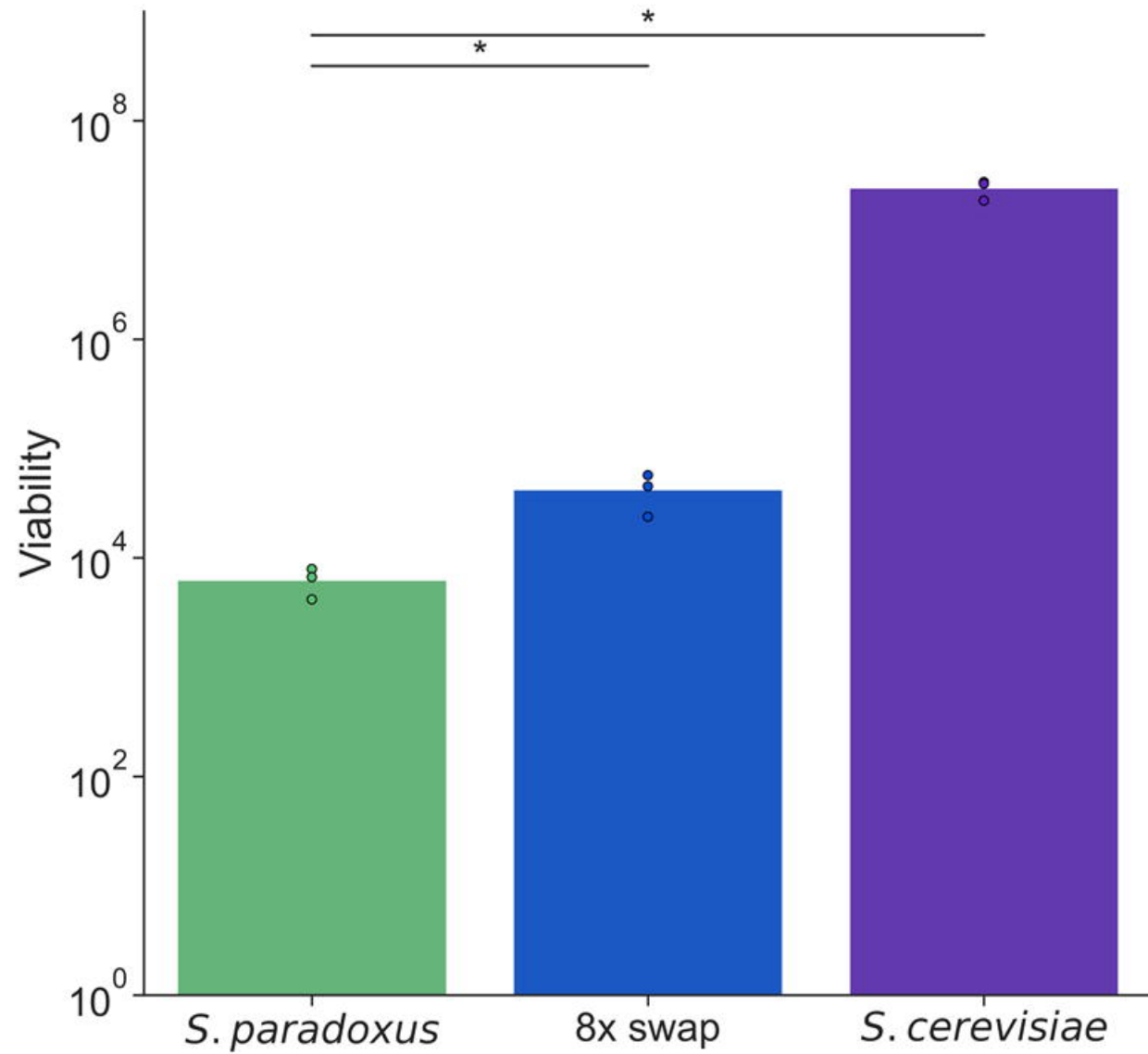
709 **Figure S9. Allelic variation at thermotolerance loci has little impact on viability at 4°C.** Data and symbols
710 are as in Figure 3A of the main text, except that liquid incubations were at 4°C, and measurements were taken
711 at day 8 of the growth timecourse. *, One-sided Wilcoxon $p \leq 0.05$.



	<i>S. paradoxus</i>	1x swap	2x swap	3x swap	4x swap	5x swap	6x swap	7x swap	8x swap
<i>DYN1</i>	●	●	●	●	●	●	●	●	●
<i>MYO1</i>	●	●	●	●	●	●	●	●	●
<i>SCC2</i>	●	●	●	●	●	●	●	●	●
<i>APC1</i>	●	●	●	●	●	●	●	●	●
<i>AFG2</i>	●	●	●	●	●	●	●	●	●
<i>ESP1</i>	●	●	●	●	●	●	●	●	●
<i>CEP3</i>	●	●	●	●	●	●	●	●	●
<i>TAF2</i>	●	●	●	●	●	●	●	●	●

● *S. paradoxus* allele
 ● *S. cerevisiae* allele

A**B**

A**B**